LIMNOLOGY and OCEANOGRAPHY

ASLO

Limnol. Oceanogr. 68, 2023, 1269–1284

doi: 10.1002/lno.12345

The role of irradiance in controlling coralline algal calcification

Erik C. Krieger [1*,a] **Wendy A. Nelson** [2,3] **Johan Grand** [4,5] **Eric C. Le Ru** [4] **Sarah J. Bury,** [3] **Amelie Cossais,** [1] **Simon K. Davy** [1] **Christopher E. Cornwall** [1]

[1]School of Biological Sciences, Victoria University of Wellington, Wellington, New Zealand
[2]School of Biological Sciences, University of Auckland, Auckland, New Zealand
[3]National Institute of Water and Atmospheric Research, Wellington, New Zealand
[4]School of Chemical and Physical Sciences, Victoria University of Wellington, Wellington, New Zealand
[5]Université de Paris, ITODYS, Paris, France

Abstract

Coralline algae are an essential element of benthic ecosystems throughout the ocean's photic zone. Yet, the role of light in shaping the physiology of coralline algae from cold-water, low-light habitats is poorly understood. Here, we assess the calcification physiology of five cool temperate coralline algae in response to different irradiance levels over 3 months. We show that in contrast to current models focused on warmer water species, previously observed enhancement of calcification rates by photosynthesis is largely limited to lower irradiances, and that the removal of CO_2 from the calcifying fluid is not the underlying mechanism of this enhancement. Instead, this most likely occurs via two processes: (1) increased ion pumping rates to elevate the calcium carbonate saturation state in the calcifying fluid; and (2) a higher daytime pH in the diffusion boundary layer that raises calcifying fluid pH. However, as irradiance increases, ion pumping becomes increasingly saturated limiting further enhancements. Our results also suggest the existence of two calcification strategies in coralline algae and indicate that magnesium incorporation is determined by the magnesium to calcium ratio in the calcifying fluid ($[Mg]_{CF}/[Ca]_{CF}$). This study adds to our mechanistic understanding of calcification in coralline algae and fills in much needed knowledge about the role of light in controlling their physiology.

Coralline algae are a diverse, cosmopolitan group of calcifying macroalgae (Rhodophyta) that are among the most crucial ecosystem engineers and foundation taxa in the ocean's photic zone (Nelson 2009). The reef systems and rhodolith beds that are created, supported, and maintained by coralline algae provide habitat and nursery ground for countless other algal, invertebrate, and fish species (Kamenos et al. 2004*a*,*b*; Nelson et al. 2014). Chemical cues produced by coralline algae are essential for the settlement and morphogenesis of numerous marine invertebrate larvae (e.g., corals, abalone, sea urchins) (Pearce and Scheibling 1991; Morse and Morse 1996; Roberts et al. 2004). As primary producers and calcifiers, coralline algae not only form the base of many marine ecosystems, but also play a crucial role in local and global nutrient cycles and the long- and short-term storage of carbon (Chisholm 2003; Bensoussan and Gattuso 2007; van der Heijden and Kamenos 2015). However, the ability of coralline algae to fulfill their fundamental ecological roles is threatened by global change, particularly ocean acidification that is projected to reduce their calcification and inhibit recruitment (Comeau et al. 2013; Kroeker et al. 2013; Ordoñez et al. 2017). The impacts of ocean acidification have been intensively researched and there is an improving understanding of how seawater pH and carbonate chemistry drive coralline algal calcification (Cornwall et al. 2017, 2018; Comeau et al. 2018). Such a comprehensive mechanistic understanding, however, is severely lacking for other environmental parameters, including key factors such as light. This is surprising, given the large suspected and reported influence of light on photophysiology and calcification rates. Furthermore, light not only moderates other global

*Correspondence: erik.krieger@kaust.edu.sa

Additional Supporting Information may be found in the online version of this article.

[a]Present address: Red Sea Research Center, King Abdullah University of Science and Technology, Thuwal, Saudi Arabia

Author Contribution Statement: E.C.K., C.E.C., W.A.N., S.K.D. designed the research. E.C.K. wrote the paper. E.C.K., A.C., and C.E.C. ran the experiment. E.C.K. and W.A.N. conducted morphological and molecular species identification. E.C.K. performed the statistical analysis. E.L.R., J.G., and S.J.B. contributed reagents/materials/analysis tools. All authors edited the manuscript, or provided intellectual input, and agreed to its submission.

change drivers such as ocean acidification, but its quality and quantity have decreased substantially due to anthropogenic activities in many locations (Benedetti-Cecchi et al. 2001; Airoldi 2003; Gorgula and Connell 2004). This is an environmental issue likely to become more widespread and intense in many coastal areas, especially near urban centers (Beck and Airoldi 2007; McGranahan et al. 2007). Understanding the role of light in driving coralline algal calcification is thus of paramount importance if we wish to predict changes in the distribution and function of these important foundational species.

It is widely recognized that increased light (and hence photosynthesis) drives increased calcification in many photoautotrophic calcifiers. This stimulating effect of light on calcification in coralline algae was identified in the early 1960's, when it was discovered that calcification is much higher during the day than at night (Goreau 1963). Many subsequent studies have confirmed this, and it is now well established that the calcification of coralline algae is light-enhanced and thus usually correlates well with irradiance and photosynthetic rate (Borowitzka 1981; Borowitzka and Larkum 1987; Martin et al. 2013*a*). At night, calcareous structures of coralline algae tend to dissolve due to the release of respiratory carbon dioxide (CO_2) which decreases pH at the surface of the thallus within the diffusion boundary layer (Borowitzka 1981; Hurd et al. 2011; Cornwall et al. 2013). The daytime increase in pH on the alga's surface, on the other hand, is the result of the removal of CO_2 (and/or bicarbonate [HCO_3^-] + hydrogen ions [H^+]) during photosynthesis (Hurd et al. 2011; Cornwall et al. 2013). This is thought to be the main driver of light-enhanced calcification, as it creates favorable conditions for calcification by elevating the saturation state (Ω) and/or carbonate ion concentration ([CO_3^{-2}]) at the surface of the alga, with inference that perhaps this also occurs at the site of calcification (Borowitzka 1981; Cornwall et al. 2014; Comeau et al. 2019*b*). However, for better studied taxa such as coccolithophores and corals, we know that light-enhanced calcification could also be the result of other processes. For these organisms, calcification is likely enhanced at higher irradiances by elevated pH, dissolved inorganic carbon (DIC) and Ω at the site of calcification via pumping protons (H^+) out, and HCO_3^- and calcium ions (Ca^{+2}) into the calcifying fluid (Allemand et al. 2004; Liu et al. 2018; Comeau et al. 2019*a*). In this scenario, increasing photosynthesis would supply increased energy to allow for light-enhanced calcification (Chalker and Taylor 1975; Allemand et al. 2004; Holcomb et al. 2014).

Here, we explore the calcification physiology and photophysiology of five coralline algal morpho-types as they respond to increasing light levels. For shallow subtidal coralline algae, we hypothesize that: (1) increased light will increase both photosynthetic and calcification rate. We also surmise that there are two most likely reasons for this occurring: elevated pH of the calcifying fluid and/or increased calcium pumping, as seen in corals (Comeau et al. 2019*a*). We therefore also hypothesize that, (2) any increase in the calcification rate will be associated with increased saturation state of the calcifying fluid. However, under rapid calcification, the depletion of the internal calcium pool has been observed in both corals and coralline algae, which might lead to the incorporation of additional magnesium into the skeleton. Thus, we also hypothesize that, (3) if under high growth, calcium demand outstrips supply, we will see an increase in the skeletal magnesium content. If high light causes photoinhibition and/or damage, we hypothesize that, (4) this will be reflected in a decreased photosynthetic rate, calcifying fluid saturation state and calcification.

To test our hypotheses on the role of light on calcification physiology, we combined standard physiological methods with Raman spectroscopy, to assess the effects of four irradiances (daily doses 0.6, 1.2, 1.8, and 2.3 mol photons m^{-2} d^{-1}) on the calcification rate, magnesium content and full-width-half-maximum (an approximation of calcifying fluid Ω) of five temperate coralline algal species/species complexes with differing morphologies. Also, we measured associated photophysiology to assess whether extremes in light (too high or too low) could cause stress, which would be apparent by reduced pigment content and biologically relevant decreases in photosynthetic efficiency, measured by the "variable fluorescence (Fv) normalized to maximal fluorescence (Fm)" parameter (Fv/Fm). We measured these parameters to explain changes in calcification physiology. Due to a substantive literature on the role of light on photophysiology, we stress here that the principal aim of our study was to elucidate the relationship between irradiance and calcification physiology.

Materials and methods

Sample collection and field sites

Coralline algae were collected 10 d prior to the experiment at depths between 1 and 2 m from two field sites located in Te Moana-o-Raukawa Cook Strait, Te Whanganui a Tara Wellington, Aotearoa New Zealand (Site A/Sharks Tooth 41°20′55.7″S, 174°47′25.8″E; Site B/Breaker Bay: 41°20′26.2″S, 174°49′32.2″E; also *see* Fig. 1) using self-contained underwater breathing apparatus. The two sites host a comparable density and diversity of macroalgae and are thus also likely very similar regarding exposure (i.e., wind and wave action) as well as the underwater light field. Since morphological identification of coralline algae is notoriously difficult, divers were instructed to collect five morphologically distinct groups that a priori we considered most likely to be species or species complexes. These included three groups of non-geniculate ("thick" = *Phymatolithopsis repanda*, $N = 37$; "smooth" = *Pneophyllum* spp., $N = 37$; and "foliose" = *Lithophyllum carpophylli*, $N = 48$), as well as two groups of geniculate corallines ("fine" = *Corallina* spp., $N = 39$; and "robust" = *Arthrocardia* spp., $N = 38$). Taxonomic consistency of collected material was examined in the laboratory before the start of the experiment using morpho-anatomical characteristics and after the experiment using molecular tools

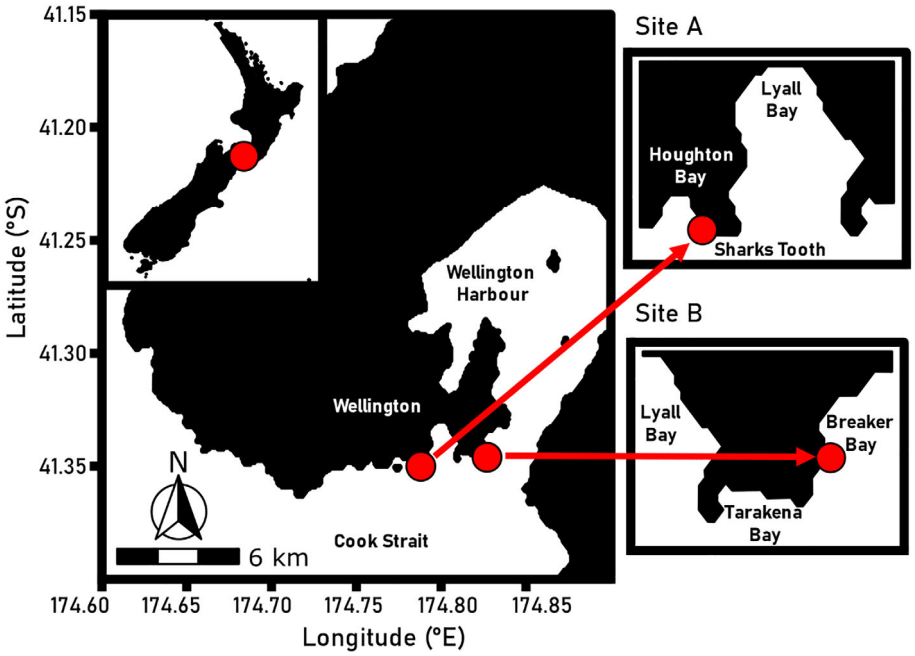

Fig. 1. Map showing the location of sampling sites A/Sharks Tooth and B/Breaker Bay, both located in Te Moana-o-Raukawa Cook Strait, Te Whanganui a Tara Wellington, at the southern end of Aotearoa New Zealand's North Island.

(for details *see* Species identification). For collection, geniculate corallines were chiseled from the rock, retaining the attached crust to avoid damaging them. Cobbles or rocks covered with thick or smooth crusts were collected directly from the seafloor. The foliose coralline, *L. carpophylli* (Heydr.) Heydr., was collected by using garden scissors to cut pieces (~ 5 cm length) of *Carpophyllum maschalocarpum*, which were overgrown by this epiphytic foliose crust that encircles *Carpophyllum* stipes. All samples were placed in separate zip lock plastic bags filled with seawater that were then placed in black plastic bags to reduce light stress and prevent physical damage, before bringing them to the surface. After collection, organisms were transported to the laboratory facilities within 20 min in cooler bins filled with ice and cool packs to further minimize thermal and light stress. At the laboratory, organisms were kept under low light levels (daily dose 0.06–0.23 mol photons m^{-2} d^{-1}) for 2 d to allow for slow acclimation to laboratory conditions. Subsequently, organisms were carefully physically cleaned of epibionts and labeled according to the morpho-anatomic classification. Epoxy (Z-Spar A-788 Splash Zone) was used to form a base for geniculate coralline algae and to cover crusts of other species on cobbles/rhodoliths. Specimens were then distributed into the experimental tanks. Each tank contained one specimen of at least three, but up to five, different species. Slow acclimation to experimental conditions was achieved by the stepwise increase of irradiance over the course of 10 days. The experiment ran from the 17 February 2019 to the 13 May 2019 (85 d).

Species identification

To verify the taxonomic consistency of the species groups recognized using morph-anatomical characters, four specimens of each species (~ 10% of total samples) were randomly selected for DNA-based identification. This was done for all species except *L. carpophylli*, where morphological identification is considered to be reliable due to its unique growth form and host specificity (Farr et al. 2009).

For identification, DNA was extracted from silica-dried samples using the Qiagen DNeasy Blood and Tissue DNA Extraction Kit (Qiagen GmbH) following the manufacturer's instructions and the protocol established by Twist et al. (2019), with the only exception that samples were ground in 200 μL AL buffer with micro-pestles. For species identification, the *psb*A marker was amplified and sequenced. Amplification of the marker was achieved by using one of two primer mixes (*psb*AF1/*psb*AR1 or *psb*AF1/*psb*AR2) (Yoon et al. 2002). The amplification protocol followed Twist et al. (2019) with the exception that each polymerase chain reaction (PCR) contained 3 μL of 5 : 95 diluted DNA extract. Quality and size of the PCR product was checked by gel electrophoresis (1% agarose). Products were then purified using ExoSAP-IT (Affymetrix Inc.) and subsequently sequenced by Macrogen. All products were sequenced in both directions. Sequences were imported into Geneious Prime 2019.2.3 (Biomatters, Ltd.), trimmed and aligned to generate a consensus sequence. These were then blasted against the National Center for Biotechnology Information (NCBI) GenBank using the "blastn" function (https://blast.ncbi.nlm.nih.gov/) to check species identity. The results from the molecular identification

enabled the creation of species groups, allowing for the correct and standardized interpretation of the results. The sequences obtained were compared to the findings of Twist et al. (2019) and showed that none of the four groups was consistently identified to the species level using morpho-anatomic characteristics, reflecting the well-known difficulties of this approach (Twist et al. 2019, 2020). Species codes below follow Twist et al. (2019) and are based on sequence data and herbarium voucher material. Representative material has been deposited in the herbarium of the Museum of New Zealand Te Papa Tongarewa, Wellington, New Zealand (WELT). Samples previously grouped under *Pneophyllum* spp. contained two Corallinales species (~ 75% *Pneophyllum* sp. F and ~ 25% *Corallinales* sp. E). Similarly, *P. repanda* samples contained two species of Hapalidiales (*P. repanda*) (= *Hapalidiales* ZT ~ 75% and *Hapalidiales* sp. D ~ 25%). The robust geniculate grouped as *Arthrocardia* spp. was revealed to consist of *Corallina* sp. (~ 75%) and *Arthrocardia* sp. B (~ 25%). The same result was obtained for the fine geniculate *Corallina* spp. (*Corallina* sp. ~ 75%/*Arthrocardia* sp. B ~ 25%). The following five groups/species (Fig. 2) will thus be used in the remainder of the text: smooth crust → *Pneophyllum* complex; thick crust → *Phymatolithopsis* complex; *Corallina*/*Arthrocardia* "fine"; *Corallina*/*Arthrocardia* "robust" and *L. carpophylli*.

Experimental treatments and design

The study was conducted at the Victoria University Coastal Ecology Lab located on Wellington's Cook Strait coastline. The experiment consisted of four different treatments each representing different light levels (daily doses 0.6, 1.2, 1.8, 2.3 mol photons m^{-2} d^{-1}). Levels were initially informed by subcanopy irradiances from other kelp forests in New Zealand (Tait et al. 2014) with their relevance for our site later confirmed by field data (Fig. 3). Each light level was replicated at the tank level 12 times for a total of 48 experimental tanks. Six experimental tanks (~ 4 L each; 17.5 cm W × 23 cm L × 12 cm H) were organized together in one 60 L water bath (56 cm W × 76 cm L × 18.5 cm H). Thus, a total of eight water baths were used to accommodate all the experimental tanks that would subsequently be treated appropriately during statistical analyses. Each water bath contained between one to two experimental tanks from each treatment (*see* Supporting Information Fig. S1). The location and number of tanks per treatment within the water bath alternated sequentially between the eight water baths for equal distribution of the experimental tanks over the whole setup. Water baths themselves were distributed over two shelf levels due to logistical constraints.

Experimental conditions

Light

Light was provided by 72 W light emitting diode panels (Zeus 70, Shenzhen Ledzeal Green Lighting Co., Ltd) mounted over each water bath. The light panels followed a natural diel cycle and were designed to mimic a natural coastal underwater light spectrum (Tait et al. 2014) (Fig. 4b). Light increased gradually in two steps (06:30 h to 09:30 h and 09:30 h to 12:30 h) to reach maximum light levels over noon (12:30 h to 16:30 h) and decreased again in two steps (16:30 h to 18:30 h and 18:30 h to 20:30 h). Different light levels in the individual tanks were achieved by covering them with coated metal

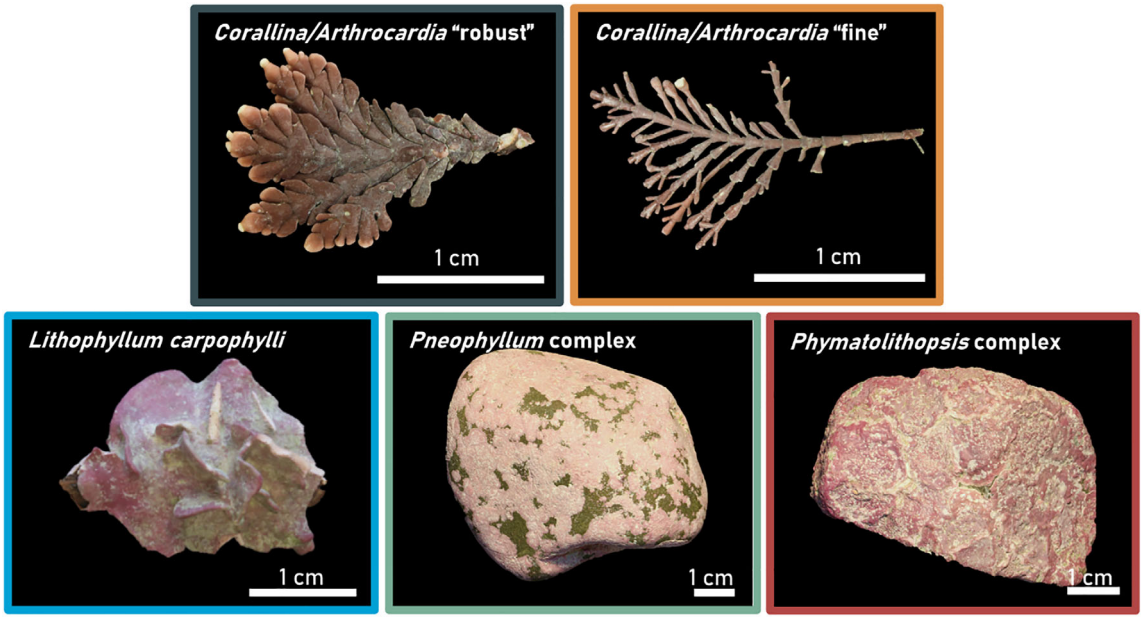

Fig. 2. Pictures showing the morphology of the five study species/species complexes. Colors associated with each morphology will be used in various figures throughout the remainder of the text.

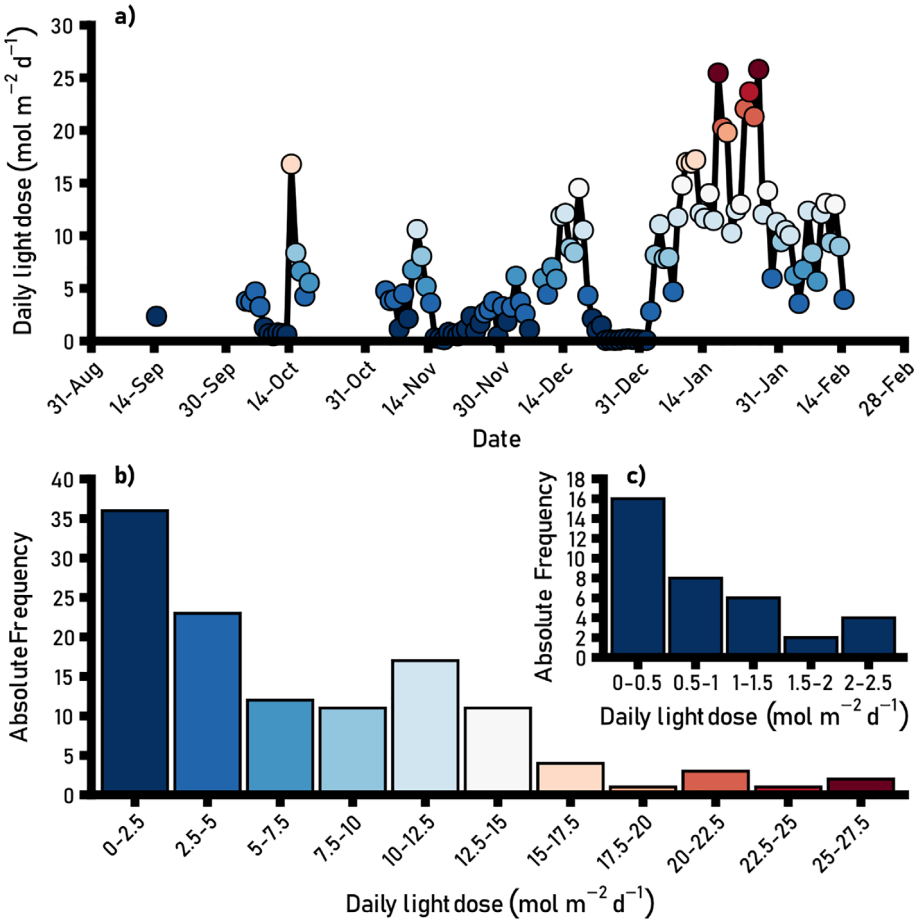

Fig. 3. (**a**) Daily light dose (mol photons m^{-2} d^{-1}) below the kelp canopy at field site A/Sharks Tooth measured over the 2020/21 New Zealand summer (mid-September 2020–mid-February 2021; $N = 117$). (**b**) Absolute frequency of daily light doses measured over this period grouped in categories. (**c**) Absolute frequency of low light events (daily light doses 0–2.5 mol photons m^{-2} d^{-1}) which were measured on ~ 30% of all days. The light levels chosen for this experiment would fall into the categories 0.5–1, 1–1.5, 1.5–2, and 2–2.5, respectively. Logging interval of integrating light loggers was set to 5 min.

mesh and various types of shade cloth. Light levels were checked regularly using an underwater photosynthetically active radiation meter (Apogee MQ-510; Apogee Instruments, Inc.) and light loggers (HOBO MX2202; Onset Computer Corporation calibrated against Apogee MQ-510) (results *see* Supporting Information Table S1).

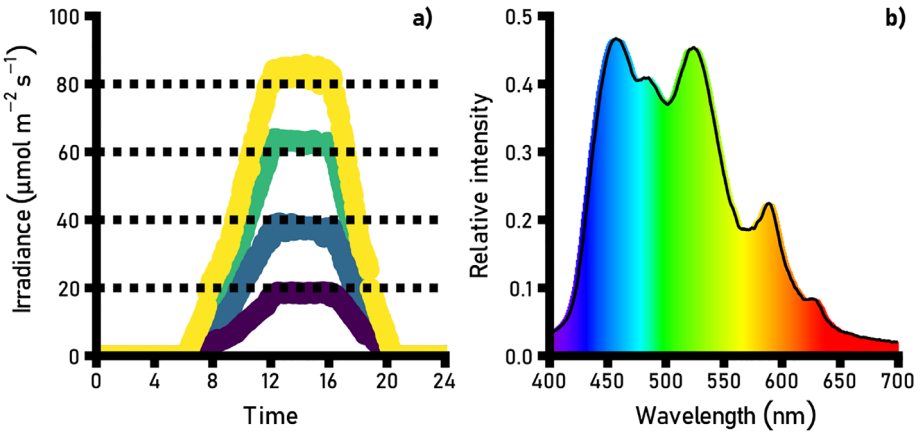

Fig. 4. (**a**) Light levels measured during a 24 h cycle in four of the experimental tanks with colors indicating treatments (color code *see* Supporting Information Fig. S1). (**b**) Spectrum of light panels used in the experiment.

Seawater supply

The seawater used for the experiment was pumped directly from the shore in front of the laboratory facilities, sand-filtered (mesh size 10 μm) and then fed into the setup. Seawater was first passed through aquarium chillers to create a baseline temperature. Chilled water was collected in two intermediate tanks (one per shelf level with $\sim$ 60 L in each; 56 cm W $\times$ 76 cm L $\times$ 18.5 cm H) and pumped from there into the header tanks ($\sim$ 20 L in each; 30 cm W $\times$ 25 cm L $\times$ 38 cm H) using submersible pumps (Jeboa DC-650; 200 L h^{-1}). There were a total of eight header tanks, and one header tank supplied each of six experimental tanks with 150 mL seawater per minute. These were equally distributed over two neighboring water baths (three per water bath). Header tanks contained one pump (Jeboa DC-650; 650 L h^{-1}) for strong water mixing. To ensure sufficient water motion around the organisms, each experimental tank was equipped with a smaller pump (Hailea BT-100; 150 L h^{-1}).

Seawater carbonate chemistry

Seawater pH, temperature and total alkalinity were measured in each header tank and in randomly selected experimental tanks of each water bath each week to assess long- and short-term variability of these parameters (results *see* Supporting Information Table S1). The pH was measured using a pH meter (HQ40D equipped with IntelliCal PHC101 probe, Hach Company) calibrated on the total scale using Tris/HCl buffers (following Dickson et al. 2007). Total alkalinity was calculated with a modified Gran function (Dickson et al. 2007). Regular titrations (AS-ALK2; Apollo SciTech) of certified reference material (Batch 176 provided by A.G. Dickson lab) yielded total alkalinity values within $\pm$ 6 μmol kg^{-1}. Seawater carbonate chemistry was calculated with the "seacarb" package running in R (R Core Team 2021).

Physiological measurements

Mean-net calcification

Mean-net calcification rates were quantified using the buoyant weight technique (Jokiel et al. 1978). The difference in weight at the start and end of the experiment was converted into dry weight of calcite and used to calculate net calcification. Net weight changes were transformed into calcification rates (mg $CaCO_3$ cm^{-2} d^{-1}) by normalizing for time of the experiment (in days) and surface area (in cm^2, for details *see* Determination of surface area). To ensure the correct calculation of calcification rate for geniculate corallines, the weight of the epoxy bases had to be subtracted. Therefore, bases were weighed after the experiment following the complete removal of the algae, and the obtained weight was subtracted from the individual sample weight from each timepoint. Due to an increase in mortality of the epiphytic *L. carpophylli* and the epilithic *Pneophyllum* complex in the second half of the experiment, calcification rates for these species are based on the weight change of healthy specimens from the first half of the experiment (17 February 2019–02 April 2019, 44 d; for more details regarding the timing of measurements and analysis *see* Supporting Information Table S2).

Raman spectroscopy

Confocal Raman spectroscopy was used to determine sample minerology and approximate calcifying fluid saturation state. Measurements were conducted with a Horiba Jobin-Yvon Labram HR Raman spectroscope (Horiba France SAS) using a green 514 nm Ar-ion laser following DeCarlo et al. (2017). The measurement was carried out with an 1800 grooves per millimeter grating, a liquid-nitrogen-cooled CCD for detection, in the backscattering configuration with a long working distance objective with $\times$50 magnification and a numerical aperture of 0.5. Wavenumber calibration was achieved through the repeated analysis of a silicon substrate. Bleached skeleton samples were placed on glass slides and analyzed manually. A total of 20 individuals per species (five per treatment) were analyzed. For each individual, 15 spectra (integration 5 $\times$ 4 s) were obtained (five spectra each from three different growth margins). Low quality or contaminated spectra were excluded from the analysis. The minerology of the sample was determined by the presence and shape of two peaks. The ν1 peak (1085–1090 cm^{-1}) which is indicative for $CaCO_3$ and the shape of the ν4 peak (700–720 cm^{-1}) which indicates presence of aragonite (double peak) or calcite (single peak) (Urmos et al. 1991). Full-width-half-maximum and position of the ν1 peak were used to determine magnesium content and to approximate calcifying fluid saturation state (DeCarlo et al. 2017). Abiogenic calibrations of Perrin et al. (2016) were used to estimate mol% magnesium (Mg) after correcting for the divergence of the silicon wavenumber obtained in this study and reported by Perrin et al. (2016). The calculated magnesium content was also used to account for the effects of high magnesium content on full-width-half-maximum. Residual ν1 full-width-half-maximum was considered a proxy for calcifying fluid saturation state of high-Mg calcite.

Inorganic carbon use

Organic tissue carbon isotope values (the ratio of ^{13}C to ^{12}C, defined as $\delta^{13}C$ in units of ‰) were measured at the end of the experiment from samples taken from five individuals from each of the species and treatments. Inorganic material was removed by placing dried specimens in 1 mol L^{-1} hydrochloric acid until bubbling of material had ceased, indicating complete removal of inorganic carbon. Remaining organic tissue was washed with MilliQ water and then dried in an oven at 75°C for at least 48 h. Dry samples were ground to a fine powder with an agate mortar and pestle. Stable isotope analyses were carried out on a DELTA V Plus continuous flow isotope ratio mass spectrometer linked to a Flash 2000 elemental analyzer using a MAS 200 R autosampler (Thermo Fisher Scientific) at the National Institute of Water and Atmospheric Research Environmental and Ecological Stable Isotope Facility in Wellington, New Zealand. ISODAT (Thermo Fisher Scientific) software calculated $\delta^{13}C$ values against a CO_2 reference

gas, relative to the international standard Carrara Marble NSB-19 (National Institute of Standards and Technology [NIST]), which in turn, was calibrated against the original Pee Dee Belemnite limestone standard and was then corrected for ^{17}O. Stable isotope ratios were expressed as delta values (δ) in per mil units (‰), which represent the ratios of heavy to light isotopes within a sample (R_{sample}), relative to the ratio in an international standard ($R_{standard}$) as: $\delta = \left(\left(\frac{R_{sample}}{R_{standard}}\right) - 1\right) \times 1000$. All estimates of variance were calculated to 1 standard deviation (SD). Carbon isotope data were corrected via a two-point normalization process (Paul et al. 2007) using NIST 8573 (USGS40 L-glutamic acid; certified $\delta^{13}C = -26.39 \pm 0.09‰$) and NIST 8542 (IAEA-CH-6 Sucrose; certified $\delta^{13}C = -10.45 \pm 0.07‰$). At the start of each run, %C values were calculated relative to a laboratory reference standard of DL-Leucine (DL-2-Amino-4-methylpentanoic acid, $C_6H_{13}NO_2$, Lot 127H1084; Sigma-Aldrich) which was also run every 10 samples to monitor analytical precision and drift. An additional international standard (USGS65 Glycine; certified $\delta^{13}C = -20.29 \pm 0.04$) was run daily to check isotopic accuracy. Repeat analysis of international standards produced $\delta^{13}C$ data accurate to within 0.15‰ with a precision of 0.15‰ for international standards and 0.25‰ for an internal squid laboratory standard.

Light and dark short-term incubations

Standard closed-chamber respirometry and the alkalinity anomaly technique were combined to measure photosynthetic, dark respiration, and light and dark calcification rates. For short-term incubations, five different individuals from each species from each treatment were randomly selected. For dark incubations, only specimens from 0.6 and 2.3 mol photons m^{-2} d^{-1} treatments were selected due to logistical constraints and the lack of a detectable impact of light treatment on dark respiration rate. Specimens were placed in clear glass containers (500 mL) which were closed under water in the header tanks, carefully avoiding enclosure of air bubbles. Closed containers, also containing a stirrer bar that was separated from the organism, were then placed on a submersible stirring plate (2mag MIXdrive6; 2mag AG). This plate was placed in a water-filled tank located under a light emitting diode panel that allowed correct adjustment of light levels. Temperature control during incubations was achieved by using a chiller and a submersible heater, that were both connected to an aquarium controller. Incubations were conducted in the afternoon (between 12:30 h and 16:30 h) during the second half of the experiment (15 April 2019–03 May 2019). Dark incubations were conducted over the same period but started early in the morning before the specimens were exposed to the day's light to keep the photophysiology consistent with what was occurring at night. Incubation times were adjusted to organism size and/or light level and ranged between 1 and 2 h. Water samples and measurement of dissolved oxygen (HQ40D equipped with IntelliCal LDO101 probe; Hach Company) in header tanks were taken at the starting point. Changes in total alkalinity and dissolved oxygen were normalized for surface area, as well as water volume and incubation time, to obtain metabolic rates. Gross photosynthesis was obtained by adding average dark respiration rate (0.6 and 2.3 only) to net rate. Calcification was calculated based on the established stoichiometric relation of 2 moles total alkalinity being removed for each mole of $CaCO_3$ precipitated. Chambers only filled with seawater which were also placed on the stirrer plate during incubations served as a control. Mean changes of total alkalinity (2 μmol kg^{-1}) and dissolved oxygen (−0.1 mg L^{-1}) in control chambers were deducted from modification of these parameters caused by the organisms, but these are within measurement error.

Photosynthetic efficiency

The Fv/Fm of each individual coralline alga was measured at the start and end of the experiment using a pulse amplitude modulated (PAM) chlorophyll fluorometer (Diving PAM/R; Heinz Walz GmbH). Settings were adjusted for each species to ensure reliable results (saturation light intensity = 8 for *L. carpophylli*, *Corallina/Arthrocardia* "fine" and *Phymatolithopsis* complex; 7 for *Corallina/Arthrocardia* "robust"; 9–10 for *Pneophyllum* complex, gain = 1, damping = 2, measuring light intensity = 1, saturation pulse width = 0.8). Individuals were dark-adapted prior to each measurement for at least 30 min. Thus, measurements were only taken after 21 : 00 h and if Fo > 120.

Light curves

Effective photosynthetic capacities and light acclimation state were assessed in the second half of the experiment (15 April 2019–03 May 2019) using the PAM's rapid light curve function. Relative electron transport rates (rETR) were obtained over noon from five individuals from each species from each treatment. Individuals were exposed for 20 s to nine increasing light steps ranging from 0 to 198 μmol photons m^{-2} s^{-1}. Nonlinear models were then fitted to the data, based on least-square error calculations to determine maximum relative electron transport rate ($rETR_{max}$), light use efficiency (α or initial curve slope) and minimum saturation intensity (E_k) (after Walsby 1997).

Pigment content

Pigment content was determined from samples taken at the end of the experiment. Therefore, fresh tissue samples were taken from five individuals from each species from each treatment. Red pigments (phycocyanin and phycoerythrin) were extracted using phosphate buffer (Sampath-Wiley and Neefus 2007). Chlorophyll *a* (Chl *a*) was extracted using ethanol (Ritchie 2008). Pigment absorbance was measured with a spectrophotometer (Evolution 300, Thermo Fisher Scientific) and content was calculated after Sampath-Wiley and Neefus (2007) for red, and Ritchie (2008), for chlorophyll pigments.

Determination of surface area

Surface area of crustose species (*Phymatolithopsis* complex, *Pneophyllum* complex, and *L. carpophylli*) was determined using the aluminum foil method (Marsh 1970). The surface area of geniculate coralline algae (*Corallina*/*Arthrocardia* "fine" and *Corallina*/*Arthrocardia* "robust") was determined by establishment of a relationship between dry weight and surface area. Therefore, small pieces were cut from the thalli of silica-dried specimens. These pieces were then used to cover a 0.25 cm^2 quadrat. The pieces required to cover the quadrat were then weighed. This weight was assumed to be the weight corresponding to 0.5 cm^2 surface area, as there was photosynthetic tissue on both sides of the cut pieces. Mean weight was then doubled to get the dry weight that would correspond to 1 cm^2. Surface area of the individual specimen was calculated by dividing the calculated dry weight of that specimen (*see* Mean-net calcification) with the mean weight of 1 cm^2. Care was taken to get material from different parts (old and new growth) of the thalli to ensure a reliable relationship.

Statistical analysis

The effect of light on all measured parameters was examined using linear mixed effect models (R package "lme4") whenever possible. Light was used as a fixed effect, and water bath and header tank as random effects. Random effects were not used for respiration and dark calcification due to overparameterization. Polynomial and linear models were both fitted to the data except for $rETR_{max}$, α, and E_k, where a purely linear correlation with light was assumed. Selection between linear and polynomial models was based on their respective conditional AIC values (cAIC; R package "cAIC4") with the selected model being the one with the lowest cAIC. If no model was clearly supported (ΔcAIC < 2), the model with the higher R^2 was selected. There were two cases where we selected the unsupported model. Conditional AIC supported a polynomial model for full-width-half-maximum in *L. carpophylli*, suggesting an exponential increase of values with irradiance, which we considered illogical. We, therefore, selected the linear model. Conversely, for magnesium content in *Phymatolithopsis* complex, we selected a polynomial model despite its higher cAIC which appeared "inflated" through the inclusion of "Header" despite explaining very little variation. The packages "refit" function in fact excluded "Header" from the linear model for this reason, which resulted in a lower cAIC. Indeed, cAIC of the polynomial model was smaller upon the exclusion of "Header" in the initial model design and in connection with its higher R^2 we thus selected the polynomial model. The assumptions of normality and equality of variance were evaluated through graphical analyses of residuals using the R software package "sjPlot". Treatment effects were determined using one-way analysis of variance with p values calculated using "lmerTest". Proportions of the variation (R^2) explained by the full models were calculated using the package "MuMin". Values with considerable leverage on model output and data structure were removed solely if organism health (i.e., bleaching) or external factors could explain disparity from other values. Such external factors were problems during measurement and/or data recording. All statistical analyses were performed with R (R Core Team 2021).

Results

Mean-net calcification

Mean-net calcification of *Corallina*/*Arthrocardia* "fine", *L. carpophylli*, and *Pneophyllum* complex was significantly affected by light, while no correlation was detected for *Corallina*/*Arthrocardia* "robust" and *Phymatolithopsis* complex (Fig. 5a; Supporting Information Table S3). Average calcification rates of *Corallina*/*Arthrocardia* "fine" were up to two times greater at intermediate light intensities (0.05–0.07 mg $CaCO_3$ cm^{-2} d^{-1}) than under maximal and minimal irradiances (0.02–0.03 mg $CaCO_3$ cm^{-2} d^{-1}). Similarly, average calcification of *L. carpophylli* was seven to 20 times higher under intermediate light levels (0.10–0.13 mg $CaCO_3$ cm^{-2} d^{-1}) when compared with the lowest and highest irradiances (< 0.01–0.01 mg $CaCO_3$ cm^{-2} d^{-1}). Calcification of *Pneophyllum* complex increased linearly with light, from 0.07 to 0.17 mg $CaCO_3$ cm^{-2} d^{-1}.

Geochemistry

Full-width-half-maximum (the proxy for calcium carbonate saturation state at the site of calcification) was significantly affected by light in two of the five species (Fig. 5b; Supporting Information Table S4). In *L. carpophylli*, full-width-half-maximum increased linearly with light from 0.21 to 0.82, while in *Corallina*/*Arthrocardia* "fine" a parabolic response was observed. The saturation state proxy was lowest under intermediate light levels (0.27–0.32) and highest under minimal and maximal irradiances (0.40–0.45). Magnesium content (Fig. 5c; Supporting Information Table S5) only changed with light in two of the five species. In *L. carpophylli*, magnesium incorporation decreased with light, from 16.83% to 14.42% Mg. In *Pneophyllum* complex, magnesium content was highest under 2.3, 1.8 and 0.6 mol photons m^{-2} d^{-1} (16.26%–16.38% Mg) and lowest under 1.2 mol photons m^{-2} d^{-1} (15.37% Mg). Analyzed samples contained solely high-Mg calcite and no other minerals.

Gross photosynthetic and dark respiration rates

Gross photosynthesis was significantly affected by light levels in four of the five species (Fig. 5d; Supporting Information Table S6). Photosynthesis increased linearly with increasing light level in *Corallina*/*Arthrocardia* "robust", *Corallina*/*Arthrocardia* "fine", and *Phymatolithopsis* complex. In *Corallina*/*Arthrocardia* "fine", gross photosynthetic rate increased linearly with light from 23.05 to 95.11 μg O_2 cm^{-2} h^{-1}, while respective rates for *Phymatolithopsis* complex increased from 4.88 to 10.18 μg O_2 cm^{-2} h^{-1}. In *Corallina*/*Arthrocardia* "robust", photosynthetic rate also increased linearly from 33.53 to 60.40 μg

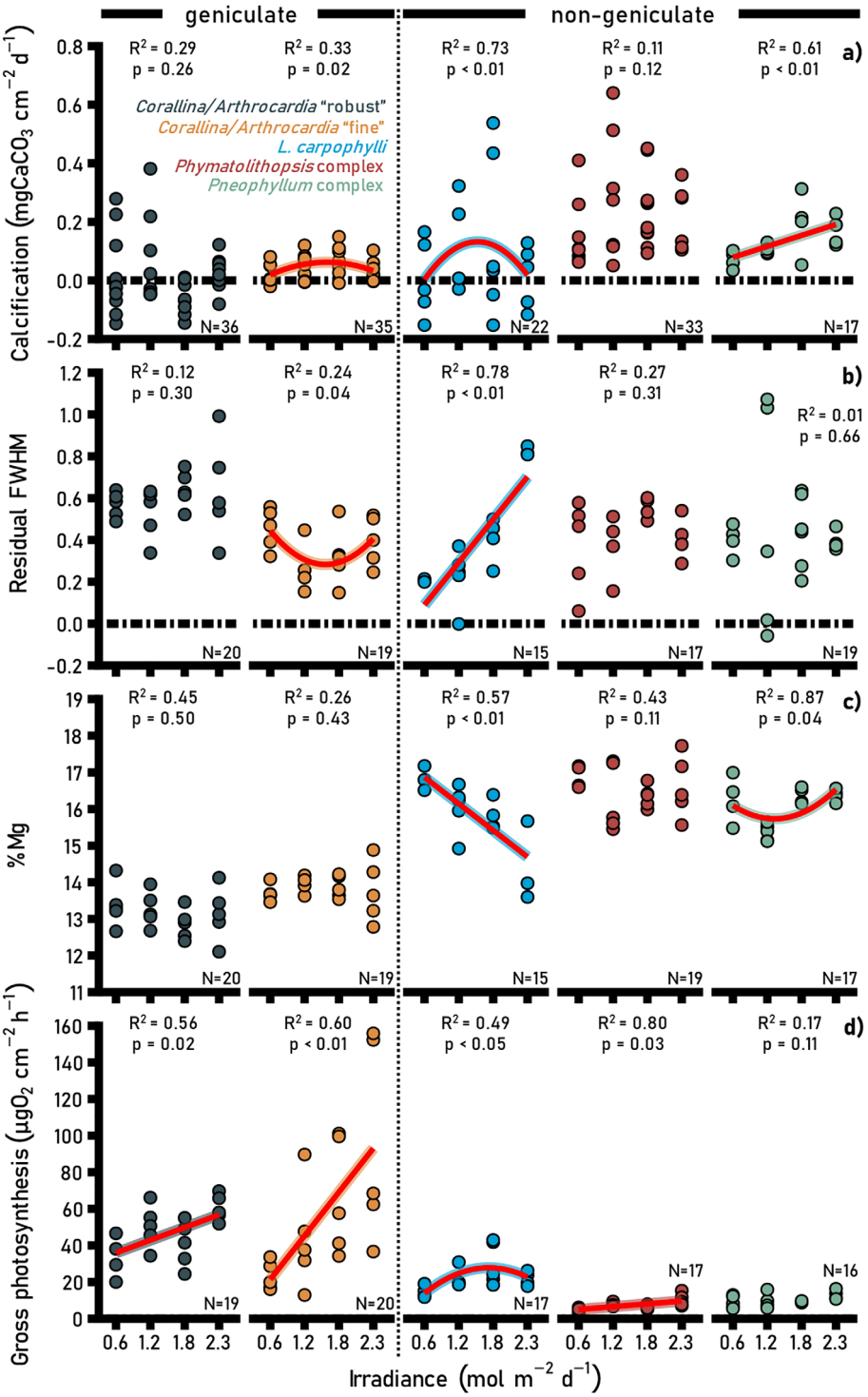

Fig. 5. Effect of irradiance on (**a**) mean-net calcification, (**b**) residual full-width-half-maximum, (**c**) magnesium content and, (**d**) gross photosynthesis of study species. Points show individual values and colors indicate species (gray = *Corallina*/*Arthrocardia* "robust"; yellow = *Corallina*/*Arthrocardia* "fine"; blue = *Lithophyllum carpophylli*; red = *Phymatolithopsis* complex; green = *Pneophyllum* complex). Lines indicate whether parabolic or linear models were fitted to the data. Proportions of variation (R^2) and probability values (*p* values) were obtained from full linear mixed effect models, and *N* = number of replicates.

O_2 cm^{-2} h^{-1}. Gross photosynthesis in *L. carpophylli* was highest under intermediate (22.12–29.79 μg O_2 cm^{-2} h^{-1}) and lowest under maximal and minimal irradiances (14.71–21.82 μg O_2 cm^{-2} h^{-1}). Dark respiration rate (*see* Supporting Information Fig. S2; Table S7) was not affected by light in any of the species.

Long- and short-term calcification as a function of full-width-half-maximum and gross photosynthesis

Mean-net calcification was not significantly correlated with full-width-half-maximum in individual specimens of any species (Supporting Information Fig. S3; Table S8). In contrast, there was a significant positive correlation between gross photosynthesis and mean-net calcification (Supporting Information Fig. S3; Table S8) in *L. carpophylli* and *Phymatolithopsis* complex but not in any of the other species. Short-term light calcification was not significantly correlated with gross photosynthesis in any of the species (Supporting Information Fig. S4; Table S9).

Carbon isotopes

The was a significant effect of light on organic $\delta^{13}C$ values (*see* Supporting Information Fig. S5; Table S10) for one of the five species. In *Pneophyllum* complex, $\delta^{13}C$ values were highest under intermediate (−23.05‰ to −20.31‰) and lowest under maximal and minimal irradiances (−23.52‰ to −24.48‰).

Light and dark calcification

Short-term light calcification was significantly affected by light in two of the five species (*see* Supporting Information Fig. S6a; Table S11). In *Pneophyllum* complex, light calcification increased linearly from −1.26 to 9.53 μg $CaCO_3$ cm^{-2} h^{-1}. In *Corallina/Arthrocardia* "robust", calcification was highest at maximal and minimal irradiances (1.15–8.22 μg $CaCO_3$ cm^{-2} h^{-1}) and lowest under intermediate light levels (−35.34 to −14.72 μg $CaCO_3$ cm^{-2} h^{-1}). Dark calcification (*see* Supporting Information Fig. S6b; Table S12) was only affected by light in *Phymatolithopsis* complex, where calcification was higher under minimum irradiances (1.99 μg $CaCO_3$ cm^{-2} h^{-1}) than under maximum irradiances (−17.79 μg $CaCO_3$ cm^{-2} h^{-1}).

Rapid light curves

Maximum saturation intensity (E_k; *see* Fig. 6; Supporting Information Table S13) and maximum relative electron transport ($rETR_{max}$; *see* Fig. 6; Supporting Information Table S13) increased with irradiance in all species (except $rETR_{max}$ in *L. carpophylli*). Light-use efficiency (initial slope of the curve or α; *see* Fig. 6; Supporting Information Table S13) only changed in *Corallina/Arthrocardia* "fine" and decreased with increased irradiance.

Photosynthetic efficiency

Photosynthetic efficiency (Fv/Fm), measured at the start and the end of the experiment, remained above 0.52 across all species and treatments (*see* Supporting Information Fig. S7).

Pigment content

Chl *a* content changed with irradiance in three of the five species (*see* Supporting Information Fig. S8; Table S14). In *Phymatolithopsis* complex, Chl *a* content was highest at the intermediate light levels (0.10–0.17 mg g^{-1}) and lowest under minimum and maximum irradiances (0.05–0.07 mg g^{-1}). In the two geniculate species, Chl *a* content increased linearly with irradiance. In *Corallina/Arthrocardia* "fine", Chl *a* content rose from 0.39 to 0.57 mg g^{-1}, while in *Corallina/Arthrocardia* "robust" the content of this pigment increased from 0.29 to 0.52 mg g^{-1}. Content of the red pigments, phycocyanin (*see* Supporting Information Fig. S8; Table S15) and phycoerythrin (*see* Supporting Information Fig. S8; Table S16), was not significantly affected by irradiance in any of the five species.

Discussion

Our results contradict our a priori hypothesis (1) that light-enhanced calcification of coralline algae is generally driven

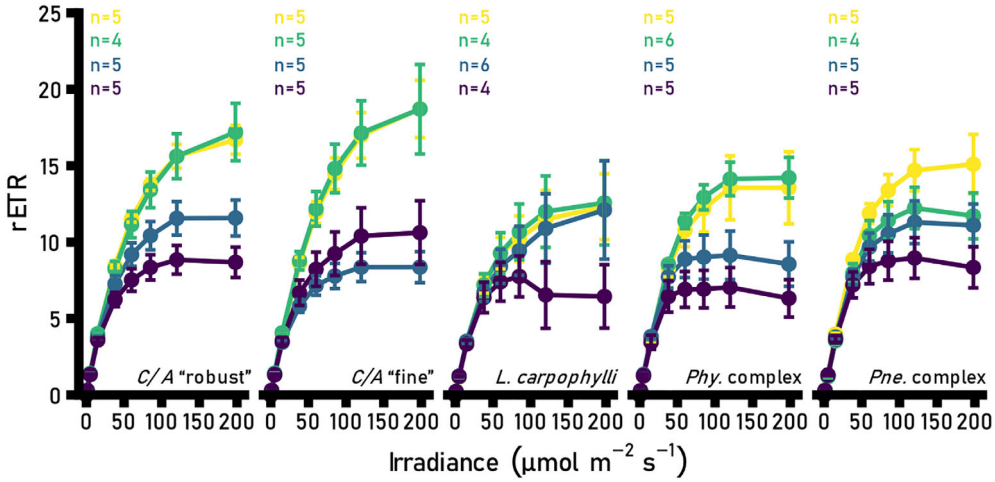

Fig. 6. Effect of irradiance on relative electron transport rates (rETR) from study species after long-term exposure to different light levels. Points show mean (± SE) and colors indicate treatments (color code *see* Supporting Information Fig. S1). Abbreviated species names represent: C/A "robust" = *Corallina/Arthrocardia* "robust"; C/A "fine" = *Corallina/Arthrocardia* "fine"; *Phy.* complex = *Phymatolithopsis* complex; and *Pne.* complex = *Pneophyllum* complex.

directly by increasing photosynthetic rate. While increasing irradiance benefits calcification here, this is limited at higher light intensities. The physiological mechanism invoked previously for light-enhanced calcification in coralline algae is that CO_2 is increasingly removed from the site of calcification for photosynthesis (Borowitzka 1981). This model necessitates that light intensity, and both photosynthetic and calcification rates are positively correlated which each other. However, this is not supported by our results. While photosynthetic rates increased with light in all but one species (parabolic in *L. carpophylli*), calcification predominantly peaked under intermediate irradiances (*Corallina*/*Arthrocardia* "fine", *L. carpophylli*, and *Phymatolithopsis* complex). Thus, only in *L. carpophylli* was calcification rate positively correlated with photosynthesis where both had a parabolic relationship. Conversely, calcification of *Corallina*/*Arthrocardia* "robust" was unaffected by light. There tended to be a positive correlation between photosynthesis and calcification for *Pneophyllum* complex, despite the increase in photosynthesis not being statistically significant. In individual samples within species (*see* Supporting Information Fig. S3) there was only a significant positive correlation between photosynthesis and calcification for *Phymatolithopsis* complex and *L. carpophylli* and no correlation was detectable for short-term calcification of any species (*see* Supporting Information Fig. S4), reflecting the overall weak link between the two metrics here for temperate low-light-adapted coralline algae. This predominance of parabolic or negligible responses of calcification to light is surprising and contradicts the findings of many earlier studies that report an increase in growth with light (Goreau 1963; Pentecost 1978; Comeau et al. 2014). Yet, there are studies that, like here, report a suppression of calcification in low-light-adapted species at high irradiances (Martin et al. 2013*b*; Egilsdottir et al. 2016). Thus, it seems logical that calcification responses to irradiance are species- and location-specific and dependent on light acclimation status, since suppression of calcification does not occur in high-light (e.g., tropical) species (Chisholm 2000). In addition, many past comparisons only assessed responses under two light regimes (e.g., high vs. low) (Martin et al. 2006; Egilsdottir et al. 2016), which excludes the detection of more complex nonlinear responses, such as the parabolic or tipping point responses identified here. Using an approach with numerous light levels enabled us to determine that faster photosynthetic rates do not always equate to faster calcification rates. In fact, calcification of low-light, temperate coralline algae can even decline as photosynthesis increases, but we note that this did not occur on the sample level, warranting further investigation.

Our findings also shed new light onto the relationship between calcification and calcifying fluid saturation state (full-width-half-maximum) in coralline algae and imply the existence of two calcification modes that coincide with two different morphologies. It is considered that coralline algae control calcifying fluid saturation state by pumping ions (Ca^{+2}, HCO_3^-) (Comeau et al. 2018) into or (H^+) (Cornwall et al. 2017) out of the calcifying fluid and facilitate calcification by elevating the fluid's saturation state (our initial a priori hypothesis 2). The same physiological mechanisms support calcification of other taxa, for example corals. However, contrary to this, we show that faster calcification coincides with low full-width-half-maximum in the two geniculate corallines. Yet, faster calcification also coincides with higher % Mg, similar to a priori hypothesis 3. Magnesium incorporation is predominantly controlled by the seawater magnesium to calcium ratio ($[Mg]_{SW}/[Ca]_{SW} \sim 5.2$) (Ries 2006), with higher ratios equating to greater magnesium content. Since this ratio was likely similar in all tanks, only changes in the species' internal ion balance ($[Mg]_{CF}/[Ca]_{CF}$) can account for the observed increase in % Mg. Therefore, it is likely that in the geniculate corallines, increased calcification outstripped the supply with calcium which elevated calcifying fluid magnesium to calcium ratios ($[Mg]_{CF}/[Ca]_{CF}$) and decreased full-width-half-maximum values, leading to the observed correlations. This is supported by similar observations made in faster growing corals and juvenile coralline algae (Ross et al. 2018; Cornwall et al. 2020). Yet, it also implies that deficiencies in calcium supply are not uncommon in marine calcifiers, a process that might impair the ability of some species to rapidly calcify (e.g., as juveniles). We speculate that some coralline algae may substitute calcium with magnesium under conditions in which a deficient calcium supply might otherwise hinder fast skeletogenesis. However, more research is required to explore the relationship between calcification rate, skeletal magnesium content and calcium supply across different taxa, as these trends were only observable in the articulate coralline algae examined here.

Calcium supply appears to exceed the demand, or is perhaps even upregulated, to facilitate growth in the non-geniculate corallines. Employment of such a strategy should create a positive correlation between full-width-half-maximum values and calcification rates and decrease % Mg. While this seems to occur in *Phymatolithopsis* complex, it is less clear for *Pneophyllum* complex and *L. carpophylli*. In *L. carpophylli*, calcification rates followed a parabola while full-width-half-maximum values increased linearly. The opposite was observed for *Pneophyllum* complex. A parabolic trend for full-width-half-maximum values in *Pneophyllum* complex is assumed despite the high variability in one treatment, potentially the result of diagenesis (Morse et al. 2006) or the inclusion of different materials (e.g., conceptacles) (Moberly 1968). The discrepancy between full-width-half-maximum values and calcification rates in these two species could be attributed to a time difference between the collection of both data sets and the normalization of calcification rate to surface area, which introduced further variation here (where surface area and full-width-half-maximum were assessed at the end of the experiment and calcification was assessed for the first half of the experiment). Indeed, uncorrected calcification rates (total gains in mg $CaCO_3$ d^{-1}, *see* Supporting Information Fig. S9; Table S17) at the end of the experiment better reflect the geochemistry

(particularly in *Pneophyllum* complex) and support the existence of two calcification modes in coralline algae. However, while two different correlations between full-width-half-maximum and calcification (positive in non-geniculate and negative in geniculate corallines) are suggested by our data, we note the absence of any correlation (positive or negative) in individual samples of both geniculate and non-geniculate corallines (*see* Supporting Information Fig. S3). In addition, there is large variability in the strength of trends across species and parameters. Thus, further examination of the relationship between full-width-half-maximum, calcification and % Mg in cool temperate coralline algae is warranted.

Based on our results we suggest that irradiance likely affects the calcification of coralline algae through a complex mix of two mechanisms: (1) increasing the supply of energy for ion pumping until energetic saturation sets in and high irradiances become stressful; and (2) increasing (via photosynthesis) and decreasing (via respiration) the pH in the diffusion boundary layer driving (daytime) precipitation and (nighttime) dissolution of $CaCO_3$, respectively. As outlined above, light-enhanced calcification is not caused by the removal of CO_2 from the calcifying fluid. We know from past research that DIC in the calcifying fluid is elevated rather than depleted in coralline algae (Comeau et al. 2018). Due to the rapid equilibrium of seawater carbonate chemistry, elevated calcifying fluid [DIC] would be impossible under a scenario of constant removal of CO_2. Yet, the correlation between diffusion boundary layer pH and pH in the calcifying fluid indicates that the removal of CO_2 from the diffusion boundary layer also elevates calcifying fluid pH (Comeau et al. 2019*b*). Here, it seems that light levels are not driving full-width-half-maximum values, yet any pH signal is most likely overwritten by changes in calcifying fluid calcium levels. Therefore, it is very likely that the removal of CO_2 from the diffusion boundary layer (but not calcifying fluid) for photosynthesis does contribute toward higher daytime-calcification rates in coralline algae. However, as daytime calcification and photosynthesis increase with irradiance, the release of respiratory CO_2 at night lowers diffusion boundary layer pH and increases $CaCO_3$ dissolution. This increase in dissolution at some point equals daytime $CaCO_3$ accretion (peak of the calcification curve) and then surpasses it (decline in mean net calcification). Indeed, mean respiration (all except *L. carpophylli*) and dissolution rate (all except *L. carpophylli* and *Pneophyllum* complex) were generally elevated at high irradiance. Yet, diffusion boundary layer pH is not the sole controller of growth.

Ion pumping to control calcifying fluid saturation state is also likely to be extremely important in determining calcification rate. This is perhaps most easily seen in the non-geniculate corallines, where it appears that calcium pumping increased with light to support faster calcification. However, in two species, calcium pumping plateaued and then declined again at the highest irradiances, which coincided with a decrease in calcification. Since dissolution affects mean net calcification but not % Mg or full-width-half-maximum values, the drop in calcification can be, in part, attributed to a decrease in calcium pumping. The reason is unclear and warrants further examination. Yet, it is possible that supply of energy plays a role. At first, ion pumping increases with light due to the concomitant increase in available energy, then becomes saturated (peak of the calcification curve) and then declines again at the highest irradiance. At this light intensity, photoinhibition and/or damage perhaps starts to become stressful, and energy is diverted away from ion pumping to alleviate this, similar to our a priori hypothesis 4. Pigment content, chlorophyll fluorometry and oxygen evolution measurements do not indicate an increase in photoinhibition except for *L. carpophylli*, in which photosynthesis declined at the highest irradiance. However, changes in the use of DIC toward more CO_2 and less HCO_3^- occurred in some species at higher irradiances (*see* Supporting Information Fig. S5), indicating a diversion of energy from these processes that could underlie some form of physiological impairment that is not otherwise measurable.

Our study species were highly sensitive to small changes in irradiance indicating that any modification of the underwater light regime is likely to negatively impact the biology and ecology of these coralline algae. In many coastal systems, the quality and quantity of light is substantially reduced by anthropogenic activities (Benedetti-Cecchi et al. 2001; Airoldi 2003; Gorgula and Connell 2004). Our results show that even a small reduction in irradiance decreases photosynthetic output and calcification performance of coralline algae. Accordingly, we should expect decreases in coralline algal abundance and shifts in their community if human activities continue to reduce coastal light levels with negative ecological outcomes (Roberts et al. 2004; Barner et al. 2016; Parada et al. 2017). However, small reductions in irradiance could provide benefits and increase productivity due to the nonlinear nature of many responses, though we consider this much less likely. Similar benefits could be received from small increments in irradiance from decreases in canopy cover, for example. However, the partial or complete removal of the canopy very likely results in irradiance increases beyond the beneficial range. Such increases in irradiance commonly result in the replacement of subcanopy, low-light species (e.g., non-geniculate corallines) with high-light species (e.g., turf algae or geniculate corallines) (Connell 2003; Irving et al. 2004; Wernberg et al. 2020) and a reduced coralline diversity (Hind et al. 2019). While the removal of the canopy signifies a rather dramatic event (which could conceivably occur in regions with acute and/or prolonged kelp retraction), we show that already relatively small increases and decreases in light intensity are enough to elicit pronounced organismal responses. These are likely to carry over to the community and ecosystem level. Any human modification of coastal light should thus be averted since this likely exacerbates variations in light availability induced by changes in cloud cover (Anthony

et al. 2004), storm frequency/intensity (Fettweis et al. 2010; Byrnes et al. 2011; Munks et al. 2015), and sea level (Saunders et al. 2013; Davis et al. 2016). Optimal light levels on the other hand could bolster the ecosystem resilience to environmental change.

Conclusion

Results show that light-enhanced calcification of coralline algae is not a result of the removal of CO_2 from the calcifying fluid. Instead, data suggest that light-enhanced calcification is the result of an elevated diffusion boundary layer pH which raises calcifying fluid pH and the increased pumping of ions into and out of the calcifying fluid. Ion pumping is likely to be stimulated by light and perhaps energetically supported by the increasing photosynthetic output. However, the higher metabolic activity seemingly increases the release of respiratory CO_2 at night. This likely decreases the pH in the diffusion boundary layer and increases night-time dissolution that can reduce the positive effect of light on growth. This, together with any change in ion pumping, can create situations in which irradiance, photosynthesis, and growth are no longer positively correlated with each other.

Our results also indicate the existence of two different calcification modes in coralline algae which coincide with their morphology and show that magnesium incorporation is likely to be driven primarily by the magnesium to calcium ratio in the calcifying fluid ($[Mg]_{CF}/[Ca]_{CF}$). However, to validate our observations, we need to directly measure calcifying fluid [Ca], pH, [DIC], and diffusion boundary layer pH at the same time, which should be the aim of future research. Future studies should also include species from different habitats and geographic regions since they are likely to respond differently. In addition, subsequent studies should strive to examine both geniculate and non-geniculate taxa to further explore the implied differences in calcification physiology. Our observations should also be corroborated by direct measurements in the field and ecological studies should aim to measure responses of low-light species/communities to changing irradiance. In such communities, the impacts of a modified light regime appear to be disproportionate, and changes in performance, productivity, and community composition are likely to precede, rather than follow those of (iconic) high-light species. This study increases our knowledge about the calcification physiology of coralline algae and provides mechanistic insights into the role of light in calcification processes. The study demonstrates the need to better understand current and future dynamics of coastal light, as its perturbation is very likely to alter coralline algal physiology, fitness and competitive outcomes that change their communities in unpredictable ways.

Data availability statement

All relevant data can be accessed here: https://doi.org/10.5061/dryad.p2ngf1vvx.

References

Airoldi, L. 2003. The effects of sedimentation on rocky coast assemblages, p. 169–171. *In* R. N. Gibson and R. J. A. Atkinson [eds.], Oceanography and marine biology, an annual review, v. **41**. CRC Press. doi:10.1201/9780203180570-23

Allemand, D., and others. 2004. Biomineralisation in reef-building corals: From molecular mechanisms to environmental control. C. R. Palevol **3**: 453–467. doi:10.1016/j.crpv.2004.07.011

Anthony, K. R. N., P. V. Ridd, A. R. Orpin, P. Larcombe, and J. Lough. 2004. Temporal variation of light availability in coastal benthic habitats: Effects of clouds, turbidity, and tides. Limnol. Oceanogr. **49**: 2201–2211. doi:10.4319/lo.2004.49.6.2201

Barner, A. K., S. D. Hacker, B. A. Menge, and K. J. Nielsen. 2015. The complex net effect of reciprocal interactions and recruitment facilitation maintains an intertidal kelp community. Journal of Ecology, **104**: 33–43. Portico. doi:10.1111/1365-2745.12495

Beck, M., and L. Airoldi. 2007. Loss, status and trends for coastal marine habitats of Europe, p. 345–405. *In* R. N. Gibson, R. J. A. Atkinson, and J. D. M. Gordon [eds.], Oceanography and marine biology: An annual review. CRC Press. doi:10.1201/9781420050943.ch7

Benedetti-Cecchi, L., F. Pannacciulli, F. Bulleri, P. Moschella, L. Airoldi, G. Relini, and F. Cinelli. 2001. Predicting the consequences of anthropogenic disturbance: Large-scale effects of loss of canopy algae on rocky shores. Mar. Ecol. Prog. Ser. **214**: 137–150. doi:10.3354/meps214137

Bensoussan, N., and J. P. Gattuso. 2007. Community primary production and calcification in a NW Mediterranean ecosystem dominated by calcareous macroalgae. Mar. Ecol. Prog. Ser. **334**: 37–45. doi:10.3354/meps334037

Borowitzka, M. A. 1981. Photosynthesis and calcification in the articulated coralline red algae *Amphiroa anceps* and *A. foliacea*. Mar. Biol. **62**: 17–23. doi:10.1007/BF00396947

Borowitzka, M. A., and A. W. D. Larkum. 1987. Calcification in algae: Mechanisms and the role of metabolism. Crit. Rev. Plant Sci. **6**: 1–45. doi:10.1080/07352688709382246

Byrnes, J. E., D. C. Reed, B. J. Cardinale, K. C. Cavanaugh, S. J. Holbrook, and R. J. Schmitt. 2011. Climate-driven increases in storm frequency simplify kelp forest food webs. Glob. Change Biol. **17**: 2513–2524. doi:10.1111/j.1365-2486.2011.02409.x

Chalker, B. E., and D. L. Taylor. 1975. Light-enhanced calcification, and the role of oxidative phosphorylation in calcification of the coral *Acropora cervicornis*. Proc. R. Soc. B Biol. Sci. **190**: 323–331. doi:10.1098/rspb.1975.0096

Chisholm, J. R. M. 2000. Calcification by crustose coralline algae on the northern Great Barrier Reef, Australia. Limnol. Oceanogr. **45**: 1476–1484. doi:10.4319/lo.2000.45.7.1476

Chisholm, J. R. M. 2003. Primary productivity of reef-building crustose coralline algae. Limnol. Oceanogr. **48**: 1376–1387. doi:10.4319/lo.2003.48.4.1376

Comeau, S., P. J. Edmunds, N. B. Spindel, and R. C. Carpenter. 2013. The responses of eight coral reef calcifiers to increasing partial pressure of CO_2 do not exhibit a tipping point. Limnol. Oceanogr. **58**: 388–398. doi:10.4319/lo.2013.58.1.0388

Comeau, S., R. C. Carpenter, and P. J. Edmunds. 2014. Effects of irradiance on the response of the coral *Acropora pulchra* and the calcifying alga *Hydrolithon reinboldii* to temperature elevation and ocean acidification. J. Exp. Mar. Biol. Ecol. **453**: 28–35. doi:10.1016/j.jembe.2013.12.013

Comeau, S., C. E. Cornwall, T. M. DeCarlo, E. Krieger, and M. T. McCulloch. 2018. Similar controls on calcification under ocean acidification across unrelated coral reef taxa. Glob. Change Biol. **24**: 4857–4868. doi:10.1111/gcb.14379

Comeau, S., C. E. Cornwall, T. M. DeCarlo, S. S. Doo, R. C. Carpenter, and M. T. McCulloch. 2019*a*. Resistance to ocean acidification in coral reef taxa is not gained by acclimatization. Nat. Clim. Change **9**: 477–483. doi:10.1038/s41558-019-0486-9

Comeau, S., C. E. Cornwall, C. A. Pupier, T. M. DeCarlo, C. Alessi, R. Trehern, and M. T. McCulloch. 2019*b*. Flow-driven micro-scale pH variability affects the physiology of corals and coralline algae under ocean acidification. Sci. Rep. **9**: 12829. doi:10.1038/s41598-019-49044-w

Connell, S. D. 2003. The monopolization of understorey habitat by subtidal encrusting coralline algae: a test of the combined effects of canopy-mediated light and sedimentation. Marine Biology **142**: 1065–1071. doi:10.1007/s00227-003-1021-z

Cornwall, C. E., C. D. Hepburn, C. A. Pilditch, and C. L. Hurd. 2013. Concentration boundary layers around complex assemblages of macroalgae: Implications for the effects of ocean acidification on understory coralline algae. Limnol. Oceanogr. **58**: 121–130. doi:10.4319/lo.2013.58.1.0121

Cornwall, C. E., P. W. Boyd, C. M. McGraw, C. D. Hepburn, C. A. Pilditch, J. N. Morris, A. M. Smith, and C. L. Hurd. 2014. Diffusion boundary layers ameliorate the negative effects of ocean acidification on the temperate coralline macroalga *Arthrocardia corymbosa*. PLoS ONE **9**: e97235. doi:10.1371/journal.pone.0097235

Cornwall, C. E., S. Comeau, and M. T. McCulloch. 2017. Coralline algae elevate pH at the site of calcification under ocean acidification. Glob. Change Biol. **23**: 4245–4256. doi:10.1111/gcb.13673

Cornwall, C. E., S. Comeau, T. M. DeCarlo, B. Moore, Q. D'Alexis, and M. T. McCulloch. 2018. Resistance of corals and coralline algae to ocean acidification: Physiological control of calcification under natural pH variability. Proc. R. Soc. B Biol. Sci. **285**: 20181168. doi:10.1098/rspb.2018.1168

Cornwall, C. E., and others. 2020. A coralline alga gains tolerance to ocean acidification over multiple generations of exposure. Nat. Clim. Change **10**: 143–146. doi:10.1038/s41558-019-0681-8

Davis, T. R., D. Harasti, S. D. A. Smith, and B. P. Kelaher. 2016. Using modelling to predict impacts of sea level rise and increased turbidity on seagrass distributions in estuarine embayments. Estuar. Coast. Shelf Sci. **181**: 294–301. doi:10.1016/j.ecss.2016.09.005

DeCarlo, T. M., J. P. D'Olivo, T. Foster, M. Holcomb, T. Becker, and M. T. McCulloch. 2017. Coral calcifying fluid aragonite saturation states derived from Raman spectroscopy. Biogeosciences **14**: 5253–5269. doi:10.5194/bg-14-5253-2017

Dickson, A. G., C. L. Sabine, and J. R. Christian [eds.]. 2007. Guide to best practices for ocean CO_2 measurements, v. **3**. PICES Special Publication.

Egilsdottir, H., J. Olafsson, and S. Martin. 2016. Photosynthesis and calcification in the articulated coralline alga *Ellisolandia elongata* (Corallinales, Rhodophyta) from intertidal rock pools. Eur. J. Phycol. **51**: 59–70. doi:10.1080/09670262.2015.1101165

Farr, T., Broom, J., Hart, D., Neill, K., and Nelson, W. 2009. Common coralline algae of northern New Zealand: An identification guide. NIWA Information Series No. 70.

Fettweis, M., F. Francken, D. Van den Eynde, T. Verwaest, J. Janssens, and V. Van Lancker. 2010. Storm influence on SPM concentrations in a coastal turbidity maximum area with high anthropogenic impact (southern North Sea). Cont. Shelf Res. **30**: 1417–1427. doi:10.1016/j.csr.2010.05.001

Goreau, T. F. 1963. Calcium carbonate deposition by coralline algae and corals in relation to their roles as reef builders. Ann. N. Y. Acad. Sci. **109**: 127–167. doi:10.1111/j.1749-6632.1963.tb13465.x

Gorgula, S., and S. Connell. 2004. Expansive covers of turf-forming algae on human-dominated coast: The relative effects of increasing nutrient and sediment loads. Mar. Biol. **145**: 613–619. doi:10.1007/s00227-004-1335-5

Hind, K. R., S. Starko, J. M. Burt, M. A. Lemay, A. K. Salomon, and P. T. Martone. 2019. Trophic control of cryptic coralline algal diversity. Proceedings of the National Academy of Sciences **116**: 15080–15085. doi:10.1073/pnas.1900506116

Holcomb, M., E. Tambutté, D. Allemand, and S. Tambutté. 2014. Light enhanced calcification in *Stylophora pistillata*: Effects of glucose, glycerol and oxygen. PeerJ **2**: e375. doi:10.7717/peerj.375

Hurd, C. L., C. E. Cornwall, K. Currie, C. D. Hepburn, C. M. McGraw, K. A. Hunter, and P. W. Boyd. 2011. Metabolically induced pH fluctuations by some coastal calcifiers exceed projected 22nd century ocean acidification: A mechanism for differential susceptibility? Glob. Change Biol. **17**: 3254–3262. doi:10.1111/j.1365-2486.2011.02473.x

Irving, A. D., S. D. Connell, and T. S. Elsdon. 2004. Effects of kelp canopies on bleaching and photosynthetic activity of encrusting coralline algae. Journal of Experimental Marine

Biology and Ecology **310**: 1–12. doi:10.1016/j.jembe.2004.03.020

Jokiel, P., J. Maragos, and L. Franzisket. 1978. Coral growth: Buoyant weight technique, p. 529–541. *In* D. R. Stoddart and R. E. Johannes [eds.], Coral reefs: Research methods. UNESCO.

Kamenos, N. A., P. G. Moore, and J. M. Hall-Spencer. 2004*a*. Nursery-area function of maerl grounds for juvenile queen scallops. Mar. Ecol. Prog. Ser. **274**: 183–189. doi:10.3354/meps274183

Kamenos, N. A., P. G. Moore, and J. M. Hall-Spencer. 2004*b*. Small-scale distribution of juvenile gadoids in shallow inshore waters; what role does maerl play? ICES J. Mar. Sci. **61**: 422–429. doi:10.1016/j.icesjms.2004.02.004

Kroeker, K. J., R. L. Kordas, R. Crim, I. E. Hendriks, L. Ramajo, G. S. Singh, C. M. Duarte, and J.-P. Gattuso. 2013. Impacts of ocean acidification on marine organisms: Quantifying sensitivities and interaction with warming. Glob. Change Biol. **19**: 1884–1896. doi:10.1111/gcb.12179

Liu, Y. W., R. A. Eagle, S. M. Aciego, R. E. Gilmore, and J. B. Ries. 2018. A coastal coccolithophore maintains pH homeostasis and switches carbon sources in response to ocean acidification. Nat. Commun. **9**: 2857. doi:10.1038/s41467-018-04463-7

Marsh, J. A. 1970. Primary productivity of reef-building calcareous red algae. Ecology **51**: 255–265. doi:10.2307/1933661

Martin, S., M. D. Castets, and J. Clavier. 2006. Primary production, respiration and calcification of the temperate free-living coralline alga *Lithothamnion corallioides*. Aquat. Bot. **85**: 121–128. doi:10.1016/j.aquabot.2006.02.005

Martin, S., A. Charnoz, and J. Gattuso. 2013*a*. Photosynthesis, respiration and calcification in the Mediterranean crustose coralline alga *Lithophyllum cabiochae* (Corallinales, Rhodophyta). Eur. J. Phycol. **48**: 163–172. doi:10.1080/09670262.2013.786790

Martin, S., S. Cohu, C. Vignot, G. Zimmerman, and J. P. Gattuso. 2013*b*. One-year experiment on the physiological response of the Mediterranean crustose coralline alga, *Lithophyllum cabiochae*, to elevated pCO_2 and temperature. Ecol. Evol. **3**: 676–693. doi:10.1002/ece3.475

McGranahan, G., D. Balk, and B. Anderson. 2007. The rising tide: Assessing the risks of climate change and human settlements in low elevation coastal zones. Environ. Urban. **19**: 17–37. doi:10.1177/0956247807076960

Moberly, R. 1968. Composition of magnesian calcites of algae and pelecypods by electron microprobe analysis. Sedimentology **11**: 61–82. doi:10.1111/j.1365-3091.1968.tb00841.x

Morse, A. N. C., and D. E. Morse. 1996. Flypapers for coral and other planktonic larvae: New materials incorporate morphogens for applications in research, restoration, aquaculture, and medicine. Bioscience **46**: 254–262. doi:10.2307/1312832

Morse, J. W., A. J. Andersson, and F. T. Mackenzie. 2006. Initial responses of carbonate-rich shelf sediments to rising atmospheric pCO_2 and "ocean acidification": Role of high Mg-calcites. Geochim. Cosmochim. Acta **70**: 5814–5830. doi:10.1016/j.gca.2006.08.017

Munks, L. S., E. S. Harvey, and B. J. Saunders. 2015. Storm-induced changes in environmental conditions are correlated with shifts in temperate reef fish abundance and diversity. J. Exp. Mar. Bio. Ecol. **472**: 77–88. doi:10.1016/j.jembe.2015.06.006

Nelson, W. A. 2009. Calcified macroalgae—Critical to coastal ecosystems and vulnerable to change: A review. Mar. Freshw. Res. **60**: 787. doi:10.1071/MF08335

Nelson, W., R. D'Archino, K. Neill, and T. Farr. 2014. Macroalgal diversity associated with rhodolith beds in northern New Zealand. Cryptogam. Algol. **35**: 27–47. doi:10.7872/crya.v35.iss1.2014.27

Ordoñez, A., E. V. Kennedy, and G. Diaz-Pulido. 2017. Reduced spore germination explains sensitivity of reef-building algae to climate change stressors. PLoS ONE **12**: e0189122. doi:10.1371/journal.pone.0189122

Parada, G. M., E. A. Martínez, M. A. Aguilera, M. H. Oróstica, and B. R. Broitman. 2017. Interactions between kelp spores and encrusting and articulated corallines: recruitment challenges for Lessonia spicata. Botanica Marina **60**. doi:10.1515/bot-2017-0010

Paul, D., G. Skrzypek, and I. Fórizs. 2007. Normalization of measured stable isotopic compositions to isotope reference scales—A review. Rapid Commun. Mass Spectrom. **21**: 3006–3014. doi:10.1002/rcm.3185

Pearce, C. M., and R. E. Scheibling. 1991. Effect of macroalgae, microbial films, and conspecifics on the induction of metamorphosis of the green sea urchin *Strongylocentrotus droebachiensis* (Müller). J. Exp. Mar. Bio. Ecol. **147**: 147–162. doi:10.1016/0022-0981(91)90179-Z

Pentecost, A. 1978. Calcification and photosynthesis in *Corallina officinalis* L. using the $^{14}CO_2$ method. Br. Phycol. J. **13**: 383–390. doi:10.1080/00071617800650431

Perrin, J., D. Vielzeuf, D. Laporte, A. Ricolleau, G. R. Rossman, and N. Floquet. 2016. Raman characterization of synthetic magnesian calcites. Am. Mineral. **101**: 2525–2538. doi:10.2138/am-2016-5714

R Core Team. 2021. R: A language and environment for statistical computing.

Ries, J. B. 2006. Mg fractionation in crustose coralline algae: Geochemical, biological, and sedimentological implications of secular variation in the Mg/Ca ratio of seawater. Geochim. Cosmochim. Acta **70**: 891–900. doi:10.1016/j.gca.2005.10.025

Ritchie, R. J. 2008. Universal chlorophyll equations for estimating chlorophylls *a*, *b*, *c*, and *d* and total chlorophylls in natural assemblages of photosynthetic organisms using acetone, methanol, or ethanol solvents. Photosynthetica **46**: 115–126. doi:10.1007/s11099-008-0019-7

Roberts, R. D., H. F. Kaspar, and R. J. Barker. 2004. Settlement of abalone (*Haliotis iris*) larvae in response to five species of coralline algae. J. Shellfish Res. **23**: 975–987.

Ross, C. L., V. Schoepf, T. M. DeCarlo, and M. T. McCulloch. 2018. Mechanisms and seasonal drivers of calcification in the temperate coral *Turbinaria reniformis* at its latitudinal limits. Proc. R. Soc. B Biol. Sci. **285**: 20180215. doi:10.1098/rspb.2018.0215

Sampath-Wiley, P., and C. D. Neefus. 2007. An improved method for estimating R-phycoerythrin and R-phycocyanin contents from crude aqueous extracts of *Porphyra* (Bangiales, Rhodophyta). J. Appl. Phycol. **19**: 123–129. doi:10.1007/s10811-006-9118-7

Saunders, M. I., and others. 2013. Coastal retreat and improved water quality mitigate losses of seagrass from sea level rise. Glob. Change Biol. **19**: 2569–2583. doi:10.1111/gcb.12218

Tait, L. W., I. Hawes, and D. R. Schiel. 2014. Shining light on benthic macroalgae: Mechanisms of complementarity in layered macroalgal assemblages. PLoS ONE **9**: e114146. doi:10.1371/journal.pone.0114146

Twist, B. A., K. F. Neill, J. Bilewitch, S. Y. Jeong, J. E. Sutherland, and W. A. Nelson. 2019. High diversity of coralline algae in New Zealand revealed: Knowledge gaps and implications for future research. PLoS ONE **14**: e0225645. doi:10.1371/journal.pone.0225645

Twist, B. A., C. E. Cornwall, S. J. McCoy, P. W. Gabrielson, P. T. Martone, and W. A. Nelson. 2020. The need to employ reliable and reproducible species identifications in coralline algal research. Mar. Ecol. Prog. Ser. **654**: 225–231. doi:10.3354/meps13506

Urmos, J., S. K. Sharma, and F. T. Mackenzie. 1991. Characterization of some biogenic carbonates with Raman spectroscopy. Am. Mineral. **76**: 641–646.

van der Heijden, L. H., and N. A. Kamenos. 2015. Reviews and syntheses: Calculating the global contribution of coralline algae to total carbon burial. Biogeosciences **12**: 6429–6441. doi:10.5194/bg-12-6429-2015

Walsby, A. E. 1997. Numerical integration of phytoplankton photosynthesis through time and depth in a water column. New Phytol. **136**: 189–209. doi:10.1046/j.1469-8137.1997.00736.x

Wernberg, T., M. Couraudon-Réale, F. Tuya, and M. Thomsen. 2020. Disturbance intensity, disturbance extent and ocean climate modulate kelp forest understory communities. Marine Ecology Progress Series **651**: 57–69. doi:10.3354/meps13443

Yoon, H. S., J. D. Hackett, and D. Bhattacharya. 2002. A single origin of the peridinin- and fucoxanthin-containing plastids in dinoflagellates through tertiary endosymbiosis. Proc. Natl. Acad. Sci. USA **99**: 11724–11729. doi:10.1073/pnas.172234799

Acknowledgments

We thank J. Van der Sman for his assistance during collection; J. Delgado and J. Brown for their help with carbon isotope measurements; Y. Tassin for creating a R script for total alkalinity analysis; and R. D'Archino for training in molecular identification. E.C.K. and C.E.C. were supported by a Rutherford Discovery Fellowship from The Royal Society of New Zealand Te Apārangi (no. RDF-VUW1701) awarded to C.E.C. Part of the research was paid for by a grant awarded to C.E.C. and W.A.N. by the Victoria University of Wellington University Research Fund. Open access publishing facilitated by Victoria University of Wellington, as part of the Wiley - Victoria University of Wellington agreement via the Council of Australian University Librarians.

Conflict of Interest

None declared.

Submitted 13 April 2022
Revised 25 November 2022
Accepted 16 March 2023

Associate editor: David Michael Baker